Icarus 362 (2021) 114424

Contents lists available at ScienceDirect

Icarus

journal homepage: www.elsevier.com/locate/icarus

Feasibility of characterizing subsurface brines on Ceres by electromagnetic sounding

Robert Grimm [a,*], Julie Castillo-Rogez [b], Carol Raymond [b], Andrew R. Poppe [c]

[a] Planetary Science Directorate, Southwest Research Institute, USA
[b] Jet Propulsion Laboratory, California Institute of Technology, USA
[c] Space Sciences Laboratory, University of California, Berkeley, USA

ARTICLE INFO

Keywords:
Asteroid Ceres
Geophysics
Interiors
Magnetic fields

ABSTRACT

Electromagnetic sounding of Ceres can be accomplished using the solar wind as a source. The depths to a deep global brine or mud layer and shallow briny intrusions can be assessed simultaneously.

1. Introduction

Dwarf planet Ceres is the largest object in the main belt and the most water-rich object in the inner solar system (in relative abundance of water to rock). Ceres had sufficient water and silicates (including radioisotopes) to host a deep ocean in its past, leading to a layered interior structure with a high degree of aqueous alteration (Ammannito et al., 2016; Ermakov et al., 2017). The Dawn mission revealed evidence of recent and possibly ongoing geologic activity on Ceres (De Sanctis et al., 2020) and the presence of liquid was inferred below an ice-rich crust (Fu et al., 2017; Scully et al., 2020; Raymond et al., 2020). Recent brine-driven exposure of material onto Ceres' surface can be found at Occator crater (Nathues et al., 2020) and Ahuna Mons (Ruesch et al., 2016). These multiple lines of evidence for deep liquid and long-lived heat sources call for categorization of Ceres as an ocean world (Castillo-Rogez, 2020).

Determination of the depth to liquid water within Ceres—specifically below Occator crater—is one objective of a recent Planetary Mission Concept Study (Castillo-Rogez and Brophy, 2020). This sample-return mission includes a landed phase of several days, allowing the opportunity for surface geophysics to provide tighter constraints on interior water over those derived from orbit. Passive seismology could be useful, but there is insufficient information at present on the strength, distribution, and recurrence of volcanotectonic or impact seismic sources suitable for analysis by a single, short-duration station. Without large resources, active-source seismology, radar, or low-frequency electromagnetics cannot penetrate the required tens of kilometers of icy crust. However, passive low-frequency electromagnetic (EM) methods are not only tractable, but optimal for this task. First, solar-wind turbulence can provide a broad temporal spectrum for EM sounding at Ceres, as was used previously for the Moon. This is important to achieving a continuum of sounding depths. Second, water with even a small quantity of dissolved salts is a strong electrical conductor compared to ice or rock: finding conductors is the essential ability of inductive EM (e.g., the familiar metal detector). The value of inductive EM for characterizing subsurface water on Mars and Europa has been studied by Grimm (2002) and Grimm et al. (2020), respectively.

In this note, we apply the same approaches to Ceres. We describe how EM sounding can be performed and derive an error budget for a representative experiment. We specify a likely range of internal structures and evaluate their EM responses. We conclude that the distances to both a deep brine-rich reservoir and a shallow brine-filled body feeding eruptions can be determined simultaneously, and furthermore that such sounding can be implemented with high confidence and low resources.

2. Electromagnetic Sounding

A changing magnetic field induces eddy currents to flow in any body with finite electrical conductivity. These currents have secondary magnetic fields that oppose the primary, such that the net magnetic field decays with 1/e folding ("skin") depth $\sqrt{2/\mu\omega\sigma}$, where μ is the magnetic permeability, ω is the angular frequency, and σ is the electrical

* Corresponding author at: Southwest Research Institute, 1050 Walnut St. #300, Boulder, CO 80302, USA.
E-mail address: grimm@boulder.swri.edu (R. Grimm).

https://doi.org/10.1016/j.icarus.2021.114424
Received 28 September 2020; Received in revised form 17 February 2021; Accepted 3 March 2021
Available online 13 March 2021

conductivity. The skin-depth effect is the essence of EM sounding that allows frequency-dependent measurements of EM fields to be translated into conductivity as a function of depth.

Although it is possible to fit EM fields directly, solid-earth geophysics commonly translates these data to proxies that have physical meaning. Here we use the apparent conductivity σ_a, which is the conductivity of a half-space having the same response as the target. Then EM sounding can be considered in terms of using the skin-depth effect to invert $\sigma(z)$ from $\sigma_a(f)$, where z is depth and f is frequency. Alternatively, the (complex) impedance $Z(\sigma_a = \mu\omega/|Z|^2)$ can be the most descriptive when considering measurement methods: the familiar Ohm's Law $Z = V/I$ calls for two independent quantities to determine the impedance, and the same applies to EM sounding.

There are two approaches to determining σ_a or Z that are relevant to Ceres (see Grimm and Delory, 2012; Banerdt et al., 2014). The Transfer Function (TF) compares the magnetic field at a planetary surface (the sum of source and induced fields) to the distant source field. This was implemented between the Apollo 12 lunar surface magnetometer and the distantly orbiting Explorer 35 satellite (e.g., Sonett, 1982). For the case of solar-wind confinement of the induced field, $\sigma_a = |2A_T/a|^2/\omega\mu$ (Hobbs et al., 1983), where A_T is the tangential component of the ratio of the proximal to distant field measurement (the transfer function) and a is the radius of Ceres. The Galileo induction studies can be considered a special case of the TF, wherein very low-frequency source fields are known and modeled a priori (e.g., Khurana et al., 1998). It is important to recognize that if the source field is not known independently, one magnetometer is insufficient to perform EM sounding. Although the transfer-function method only requires one surface and one orbiting three-component magnetometer, the instruments should be the same or have comparable performance.

In the Magnetotelluric Method (MT), the apparent conductivity is calculated from the horizontal electric field E_x and its orthogonal magnetic field B_y: $\sigma_a = (\omega/\mu)|B_y/E_x|^2$. Because E supplies the required second piece of information, the source field does not need to be known. Vector measurements (using both B_y/E_x and B_x/E_y) further enable anisotropy, or directionality of targets, to be determined. The vector magnetic field can be determined by magnetometers at the recording station. The electric field is measured from the voltage drop V between surface electrodes separated by distance d: $E = V/d$. Typical separations are 30–100 m in terrestrial experiments in order to observe a tractable voltage, and two sets of electrodes are necessary to measure the vector horizontal electric field. MT is among the most highly developed and widely applied EM method for investigations of Earth's crust and upper mantle (e.g., Simpson and Bahr, 2005; Berdichevsky and Dmitriev, 2010; Chave and Jones, 2012).

True conductivity as a function of depth $\sigma(z)$ is recovered from $\sigma_a(f)$ by inverse methods. Occam's inversion (Constable et al., 1987) is popular, which minimizes a weighted sum of the misfit between the observed and predicted data and the sum of model roughness, typically the absolute value of the log conductivity gradient. Heuristically, the inversion can be thought of as assigning the conductivity at the highest measured frequency to the uppermost layer, and progressively solving for the conductivity at greater depths by comparing the response at the next depth to the conductivity of the overlying material. This skin-depth effect is also why EM sounding is not formally non-unique (in contrast to potential-field methods such as gravity and magnetics), although poor results can follow from incomplete data.

3. Measurement

We analyze the performance of a magnetotelluric sounder on Ceres (Fig. 1) by the same approach used by Grimm et al. (2020) for a similar instrument on Europa. The closely related Lunar Magnetotelluric Sounder has been selected for flight to the Moon in 2023 under NASA's Commercial Lunar Payload Services program. For a Ceres New Frontiers class mission, we adopt the performance characteristics of the magnetometer system described for the Solar Probe Plus FIELDS instrument (Bale et al., 2016; their Fig. 2). This includes a "full-sized" MAVEN fluxgate magnetometer (Connerney et al., 2015) instead of the compact sensor we used previously, and it adds a search coil magnetometer to extend the frequency range. The electrometer system is intrinsically broadband; its performance is derived from THEMIS (Bonnell et al., 2008) but is actually about five times better than our previous analyses because the electrodes are assumed to be separated by 100 m. This distance was derived empirically as part of this study. A spring launcher derived from the Europa design can readily deploy an electrode and connecting cable to 100 m in the low gravity of Ceres; we assume just half of that and measure the electric field from the voltage difference between oppositely deployed electrodes.

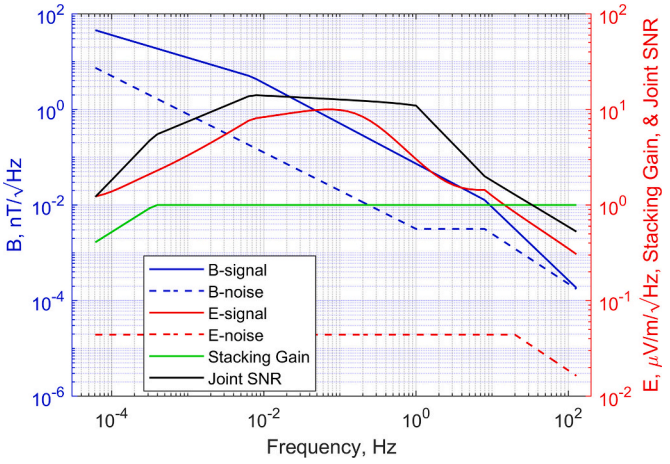

Fig. 1. Analysis of signals and noise for magnetotelluric sounding of Ceres (see text). Solar wind magnetic field mean turbulence spectrum B is scaled from 1 AU. Electric field E is calculated from the reference interior structure. Noise floors for magnetometers and electrometer are modified from FIELDS and THEMIS, respectively. Stacking gain penalizes <30 cycles over 5 Ceres days (daylight only). The joint SNR is derived from the product of the stacking gain and the sum of the variances of the two sensors, and has a median value of 10 over a bandwidth of 10 Hz.

The minimum frequency considered is 6.1×10^{-5} Hz, corresponding to one-half of Ceres 9.1-h rotation period. This assures that all measurements are made in daylight, because the electrodes rely on coupling to the environment via photoelectrons (Bonnell et al., 2008). We assume that signal integration can take place over 50 h, based on the planned duration of the landed mission (Castillo-Rogez and Brophy, 2020). The sensor noise floors are assumed to be determined with ample integration time; we impose a penalty at frequencies that are unable to achieve 30 cycles over the mission duration.

Although several spacecraft have performed interplanetary magnetic-field measurements at distances of several AU, we found no published comprehensive spectra over our full bandwidth of interest. Klein et al. (1987) found that time-averaged radial variations in large-scale magnetic field strength followed the Parker model, $B \propto \sqrt{1+R^2}/R^2$, where R is the heliocentric distance in AU. Because the square root of the integral of the power spectral density is the RMS field strength, we assume that the source magnetic field amplitude spectrum at Ceres can be approximated as the near-Earth spectrum multiplied by the Parker scale factor. We adopt the magnetic spectrum of solar wind turbulence given by Bale et al. (2016)—who used Parker scaling of spectra for the inner solar system—and derive a multiplier of 0.2725 in extrapolating the mean strength at 1 AU to 2.76 AU. We neglect temporal variations in the solar wind properties (e.g., Gonzalez-Esparza and Smith, 1996) for this initial study.

The E-field is calculated from the input B-field and the reference electrical conductivity (impedance) of Ceres as described below. This is the minimum electric field and defines the measurement requirement.

Treatment of other fields is described below. This formulation also does not explicitly treat solar-wind confinement of the induced field on the dayside (e.g., Sonett, 1982), so in fact the input B-fields are minima.

Since $\sigma_a \propto (B/E)^2$, the variance in the apparent conductivity $\varsigma^2_{\sigma a}$ follows from the variances in the electric and magnetic fields, ς^2_E and ς^2_B, respectively, as

$$\frac{\varsigma^2_{\sigma_a}}{\sigma^2_a} = 4\left(\frac{\varsigma^2_E}{E^2}+\frac{\varsigma^2_B}{B^2}\right) \quad (1)$$

The joint signal-to-noise ratio SNR = $N(\sigma_a/\varsigma_{\sigma a})$, where N is the integration gain. We find that SNR is >1 for all frequencies <30 Hz. The errors $\varsigma_{\sigma a}$ are plotted on the reference model in Figs. 2 and 3. From Fig. 1, it is evident that SNR is limited by the accuracy of the magnetic-field measurement.

By comparison, the SNR for the Apollo 12 – Explorer 35 transfer lunar transfer function (at higher ambient field levels) was ~20 over 10^{-5} to 10^{-3} Hz (Hobbs et al., 1983). However, at higher frequencies—where wavelengths in the plasma are comparable to the planetary circumference—distortions are introduced into the transfer function. While there has been some success in treating these effects up to 30 mHz (Sonett et al., 1972), the best inversions for the conductivity structure of the Moon restricted the frequency to ≤1 mHz (Hood et al., 1982; Khan et al., 2006). Assuming that the useful bandwidth scales inversely as planetary radius, plasma distortion to the transfer function at Ceres will appear >4 mHz and will be intractable >100 mHz. This will not affect the ability of TF to probe for a deep brine layer, although shallow brine conduits will be undetectable (see below).

On Ceres as on Earth, the ability to recover subsurface structure may depend on additional factors. We mentioned above that we neglect temporal variations in source-field strength; it is possible that SNR < 1 could result from anomalously low solar-wind fields during the short duration of the surface mission. Extraneous EM sources can contribute coherent or incoherent noise. Plasma waves may cause other, non-inductive fields that can be separated using the frequency-dependent amplitude and phase relations that planetary induction must satisfy. This is another benefit of broadband measurements. Artificial "cultural noise" is ubiquitous on Earth but of course will be limited to the lander itself on a Ceres mission. The electrodes are naturally distant but the magnetometers are mounted on masts or booms to increase the dipolar attenuation from the lander. We have also noted that the measurement depends on photoelectron coupling in daylight, unlike conventional grounded MT electrodes. And of course the overall quality of the inversion depends on the bandwidth and quality of the measurements. All of these effects will be evaluated for the 2023 lunar mission.

4. Modeling

We specify a series of 1D (layered) models σ(z) for Ceres and calculate the frequency-dependent apparent conductivities $\sigma_a(f)$ using the method described by Grimm and Delory (2012). This uses a cartesian recursion relation (Wait, 1970) with a spherical transformation (Weidelt, 1972) and allows an arbitrarily discretized radial conductivity structure. This model applies specifically to the dipole response of a sphere in vacuum. In reality, the solar-wind interaction with Ceres confines the dayside induced field and may also lead to a weak, comet-like signature if water vapor is present (Lindkvist et al., 2017). It is unnecessary for us to model these details at this introductory level for two reasons. First, the confinement factor for a bare Ceres can be computed from the vacuum response (see Sonett, 1982, Eq. 33 and Fig. 11), such that the magnetic fields for TF can be derived. Second, Faraday's Law still holds, so the computed E varies proportionally to the enhanced B and the MT ratio still applies. The single-station completeness of MT allows it to operate without regard to "upstream" effects of the solar wind, or for that matter an overlying ionosphere or magnetosphere. The transfer function will be further distorted by these additional plasma effects. One-standard-deviation error bars were derived from the joint errors in the electric and magnetic field measurements (MT method) described above.

The reference structure has a 35 km thick crust with conductivity 10^{-4} S/m that overlies a brine-rich layer with conductivity 1 S/m extending to 100 km depth. For convenience, we call the brine reservoir an "ocean," although it could contain substantial silicates. The crustal thickness is rounded from Ermakov et al. (2017). The crustal conductivity is the maximum DC sub-eutectic conductivity of ice formed from an NaCl-saturated solution (Grimm et al., 2008). It will be seen that this value, and hence all smaller values, have little effect on the results. The ocean conductivity is varied between 20 S/m (approximately a saturated chloride solution, CRC, 2008, p. 5–72) and 0.2 S/m (5 S/m seawater in 20% porosity, Archie's Law with cementation exponent 2), with the reference value near the logarithmic mean. Below that, a phyllosilicate mantle is assigned a conductivity of 10^{-2} S/m, representative of consolidated shale (Telford et al., 1990, p. 290).

In order to assess discrimination of shallow vs deep conductors, a briny sill (0.2 km, 0.1 S/m) is inserted at 2 km depth. This is included in the reference model and is used for all parameter studies that follow. The single layer can be considered a proxy for multiple thinner and brinier intrusions (e.g., 10 sills in series with thickness 10 m and conductivity 20 S/m). The sill is chosen for convenience in representing shallow water bodies because it can be incorporated in a 1D model. A dike is more plausible (Raymond et al., 2020; Scully et al., 2020) but requires a

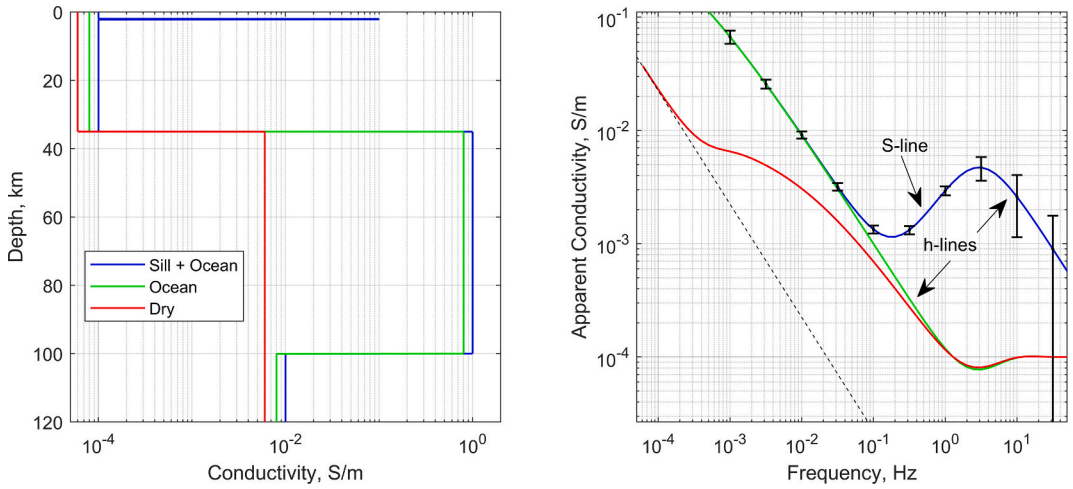

Fig. 2. Basic interior models (left, displaced for clarity) and EM responses (right) for Ceres. See text for discussion. Error bars are derived from Fig. 1.

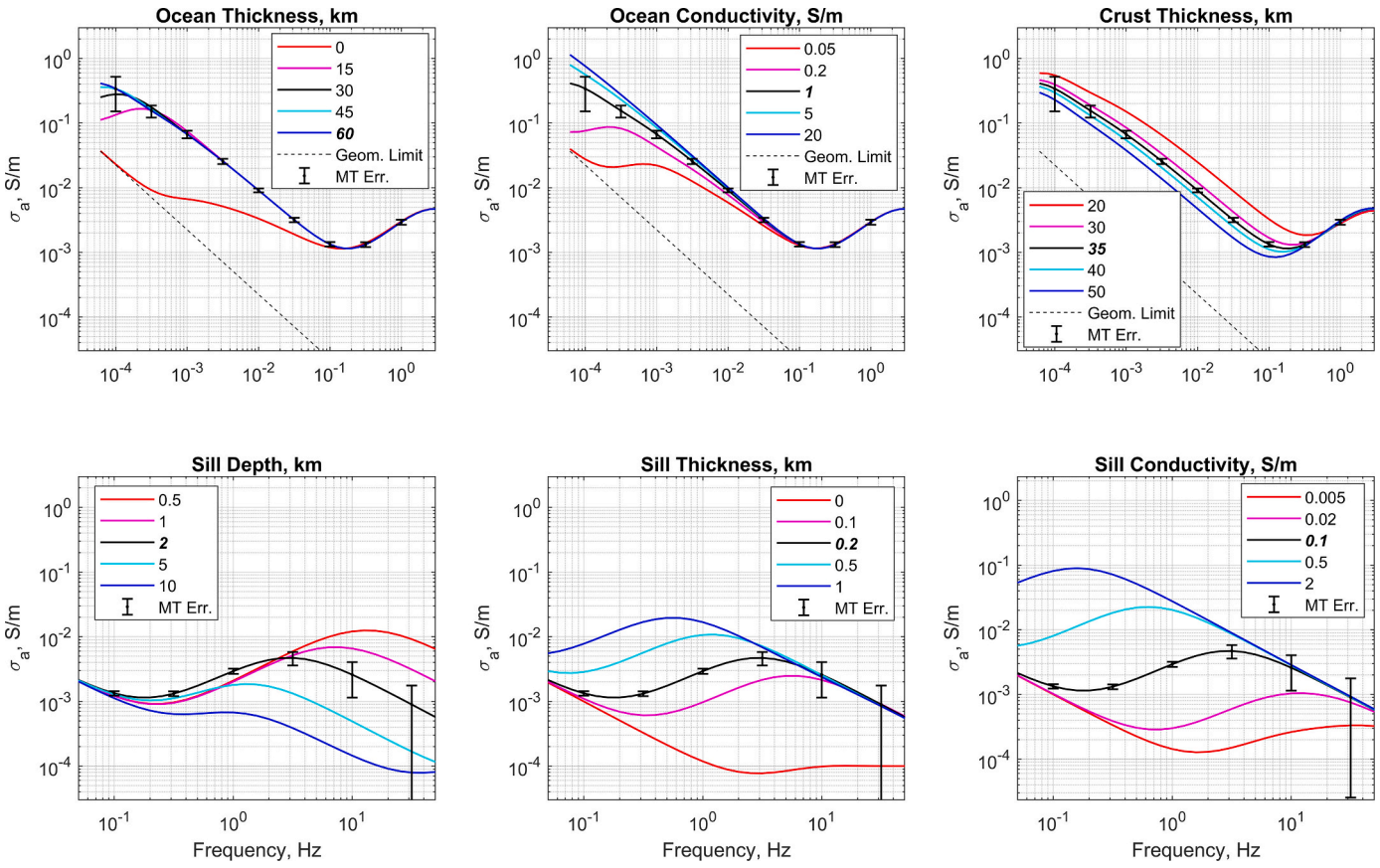

Fig. 3. Parametric study of EM sounding of Ceres. Note different abscissa ranges in top and bottom rows. Crustal thickness is well-characterized <0.1 Hz, but ocean thickness and conductivity are ambiguous. Similarly, the depth to a shallow conductor (sill) is readily measured >1–10 Hz, but only its thickness-conductivity product can be determined.

3D model: representative 3D calculations are given in the Supplementary Material. Overall, the modeled 1D structure has up to four layers: icy crust, briny sill, icy crust, and ocean.

The actual and apparent conductivities for the reference model, and for models successively deleting the sill and then the ocean, are shown in Fig. 2. First consider the dry structure (red curve). At the highest frequencies, σ_a is equal to the true conductivity of the crust. These signals are entirely absorbed in the crust. Below 1 Hz, the response trends toward a -45° log–log slope. This is diagnostic of signals that are sensing a strong conductor and follows $\sigma_a = 1/\mu\omega h^2$, where h is the depth to the conductor. For strong, thick, conductors, the depth to the conductor can be directly read off from any point on this "h-line" (Berdichevsky and Dmitriev, 2010). In this first case, however, the slope begins shallowing as lower frequencies penetrate farther into the phyllosilicate mantle and begin to asymptote toward its actual conductivity 10^{-2} S/m. Before this is fully realized, the signals have completely penetrated Ceres and σ_a trends back to another h-line that represents a geometric limit: below $\sim 3 \times 10^{-4}$ Hz, the EM response simply indicates the presence of a sphere (Ceres) in free space without any information on its composition (dashed line in Fig. 2).

When the ocean is present at the bottom of the crust (green curves), the high-frequency response to the uppermost layer is the same, but the h-line continues across four decades of frequency. Measurements anywhere along this extensive h-line are sufficient to determine the depth to brine. The EM signals do not begin penetrating into the underlying mantle until the lowest frequencies.

The full reference model with both sill and ocean (blue curves) introduces a new h-line at high frequency, whose higher apparent conductivity reveals the shallower depth of the sill. The transition between the signatures of the sill and the ocean is around 1 Hz. The segment 0.2 to 3 Hz has $+45^\circ$ log-log slope and is given by $\sigma_a = \mu\omega S^2$, where $S = \sigma H$ is the conductance of the overlying sill of thickness H. This "S-line" (Berdichevsky and Dmitriev, 2010) indicates that the conductivity and thickness of the sill cannot be determined separately. If the sill was much thicker, σ_a would asymptote to the sill's actual σ at lower frequency and the S-line could then be used to determine the sill's thickness. At lower frequencies here, the ocean's h-line signature is still evident.

In summary, the reference model broadly indicates that the ocean depth can be determined at frequencies between 6×10^{-5} and 1 Hz if no sill is present. Otherwise, the ocean's signature is still evident up to 0.3 Hz and the depth to the sill is determined above 3 Hz.

In Fig. 3, we explore the effects of six parameter variations (crust thickness, ocean thickness and conductivity, sill depth, thickness, and conductivity) from the reference model. There is little sensitivity to ocean thickness > 30 km (depth 65 km) because signals at useful frequencies are absorbed by the saltwater. Note that here the calculation for zero ocean thickness still includes the overlying sill. Ocean conductivities lower than the reference value—due to lower salt content or a higher silicate fraction—can be distinguished, but the curves for near-eutectic compositions merge as signal penetration is diminished. H-lines for the depth to the top of the ocean (crust thickness) and the depth to the top of the sill are well-developed. Test values for ocean depth are closely spaced because there are already constraints (Ermakov et al., 2017), and the small expected measurement errors in this band suggest that the shell thickness can be determined to within a few km. The families of S-lines for sill thickness and conductivity illustrate the equivalence (ambiguity) in separating these parameters.

5. Concluding Discussion

The subsurface water reservoirs of Ceres may hold important clues to the evolution, differentiation, and habitability of ocean worlds. Electromagnetic sounding is the best geophysical approach for assessing not just a large, deep, brine reservoir, but also liquid in shallow intrusions that may be the sources of recent extrusion. An orbiter with high apoapsis and a lander can together perform basic sounding using the magnetic transfer function method. However, the transfer function is likely be limited to <0.1 Hz due to plasma effects. At these frequencies, the ocean can be detected but not shallow intrusions. This method requires concurrent observations by two flight elements, which increases mission cost. In contrast, the magnetotelluric method measures both electric and magnetic fields at the lander and does not require an orbiter. It is largely insensitive to plasma effects and can distinguish different shallow intrusive structures by their anisotropic responses. A magnetotelluric instrument is baselined in the payload of a Ceres lander and sample-return mission study under consideration for the 2023–2032 Planetary Science and Astrobiology Decadal Survey.

Declaration of Competing Interest

None declared.

Acknowledgements

This work was funded by NASA grants 80NSSC17K0769 (AP) and 80NSSC19K0609 (RG). We thank Mike Sori, Simone Marchi, and David Stillman for helpful discussion and review. RG is grateful to the Europa/Lunar Magnetotelluric Sounder Team for their contributions to realizing this technique in planetary exploration.

Appendix A. Supplementary data

Supplementary data to this article can be found online at https://doi.org/10.1016/j.icarus.2021.114424.

References

Ammannito, E., DeSanctis, M.C., Ciarniello, M., et al., 2016. Distribution of phyllosilicates on the surface of Ceres. Science 353. https://doi.org/10.1126/science.aaf4279.

Bale, S.D., et al., 2016. The FIELDS instrument suite for solar probe plus. Space Sci. Rev. 204, 49–82. https://doi.org/10.1007/s11214-016-0244-5.

Banerdt, W.B., Dehant, V., Grimm, R., Grott, M., Lognonne, P., Smrekar, S., 2014. Ch. 55, Probing the interiors of planets with geophysical tools. In: Spohn, T.E. (Ed.), Encyclopedia of the Solar System, 3rd ed. Elsevier, pp. 1185–1204.

Berdichevsky, M.N., Dmitriev, V.I., 2010. Models and Methods of Magnetotellurics. Springer, Berlin, Heidelberg.

Bonnell, J., Mozer, F., Delory, G., Hull, A., Ergun, R., Cully, C., Angelopoulos, V., Harvey, P., 2008. The electric field instrument (EFI) for THEMIS. Space Sci. Rev. 141, 303–341.

Castillo-Rogez, J., Brophy, J., 2020. Planetary Mission concept study: exploration of Ceres habitability. NASA Planetary Mission Concept Studies Reports. https://science.nasa.gov/files/science-red/s3fs-public/atoms/files/Exploration%20of%20Ceres%20Habitability.pdf.

Castillo-Rogez, J.C., 2020. Comment: future exploration of dwarf planet Ceres, a newly found ocean world close to Earth. Nat. Astron. 4 (732), 734.

Chave, A.D., Jones, A.G., 2012. The Magnetotelluric Method: Theory and Practice. Cambridge University Press.

Connerney, J.E.P., Espley, J., Lawton, P., Murphy, S., Odom, J., Oliversen, R., Sheppard, D., 2015. The MAVEN magnetic field investigation. Space Sci. Rev. 1–35.

Constable, S., Parker, R., Constable, C., 1987. Occam's inversion: A practical algorithm for generating smooth models from electromagnetic sounding data. Geophysics 52, 289–300. https://doi.org/10.1190/1.1442303.

CRC, 2008. Handbook of Chemistry and Physics, 88th ed. CRC Press.

De Sanctis, M.C., Ammannito, E., Raponi, A., Frigeri, A., Ferrari, M., Carrozzo, F.G., Ciarniello, M., Formisano, M., Rousseau, B., Tosi, F., Zambon, F., Raymond, C., Russell, C., 2020. Recent emplacement of hydrated sodium chloride on Ceres from ascending salty fluids. Nat. Astron. https://doi.org/10.1038/s41550-020-1138-8.

Ermakov, A.I., Fu, R.R., Castillo-Rogez, J.C., Raymond, C.A., Park, R.S., Preusker, F., Russell, C.T., Smith, D.E., Zuber, M.T., 2017. Constraints on Ceres' internal structure and evolution from its shape and gravity measured by the Dawn spacecraft. J. Geophys. Res: Planets 122, 2267–2293.

Fu, R., Ermakov, E., Marchi, S., Castillo-Rogez, J.C., Raymond, C.A., Hager, B.H., Zuber, M.T., King, S.D., Bland, M.T., De Sanctis, M.C., Preusker, F., Park, R.S., Russell, C.T., 2017. The interior structure of Ceres as revealed by surface topography. Earth Planet. Sci. Lett. 476, 153–164.

Gonzalez-Esparza, J.A., Smith, E.J., 1996. Three-dimensional nature of interaction regions: pioneer, voyager, and ulysses solar cycle variations from 1 to 5 AU. J. Geophys. Res. 102, 9781–9792. https://doi.org/10.1029/97JA00516.

Grimm, R.E., 2002. Low-frequency electromagnetic exploration for groundwater on Mars. J. Geophys. Res. 107 https://doi.org/10.1029/2001JE001504.

Grimm, R.E., Delory, G.T., 2012. Next-generation electromagnetic sounding of the moon. Adv. Space Res. 50, 1687–1701.

Grimm, R.E., Stillman, D.E., Dec, S.F., Bullock, M.A., 2008. Low-frequency electrical properties of polycrystalline saline ice and salt hydrates. J. Phys. Chem. B 112, 15382–15390.

Grimm, R.E., et al., 2020. A magnetotelluric instrument for probing the interiors of Europa and other worlds. Adv. Space Res. arxiv https://arxiv.org/abs/2101.06730.

Hobbs, B.A., Hood, L.L., Herbert, F., Sonett, C.P., 1983. An upper bound on the radius of a highly electrically conducting lunar core. J. Geophys. Res. 88, B97–B102.

Hood, L.L., Herbert, F., Sonett, C.P., 1982. The deep lunar electrical conductivity profile: structural and thermal inferences. J. Geophys. Res. 87, 5311–5326.

Khan, A., Connolly, J.A.D., Olsen, N., Mosegaard, K., 2006. Constraining the composition and thermal state of the moon from an inversion of electromagnetic lunar day-side transfer functions. Earth Planet. Sci. Lett. 248, 579–598.

Khurana, K.K., Kivelson, M.G., Stevenson, D.J., Schubert, G., Russell, C.T., Walker, R.J., Polanskey, C., 1998. Induced magnetic fields as evidence for subsurface oceans in Europa and Callisto. Nature 395 (6704), 777–780. https://doi.org/10.1038/27394.

Klein, L.W., Burlaga, L.F., Ness, N.F., 1987. Radial and latitudinal variations of the interplanetary magnetic field. J. Geophys. Res. Space Physics 92, 9885–9892.

Lindkvist, J., Lindkvist, J., Holmström, M., Fatemi, S., Wieser, M., Barabash, S., 2017. Ceres interaction with the solar wind. Geophys. Res. Lett. 44, 2070–2077. https://doi.org/10.1002/2016GL072375.

Nathues, A., Schmedemann, N., Thangjam, G., Pasckert, J.H., Mengel, K., Castillo-Rogez, J., Cloutis, E.A., Hiesinger, H., Hoffmann, M., Le Corre, L., Li, J.-Y., Pieters, C., Raymond, C.A., Reddy, V., Ruesch, O., Williams, D.A., 2020. Recent cryovolcanic activity at Occator crater on Ceres. Nat. Astron. https://doi.org/10.1038/s41550-020-1146-8.

Raymond, C.A., Castillo-Rogez, I., Ermakov, S., Marchi, B., Johnson, R.S., Park, J.E.C., Scully, D.L., Buczkowski, A., Nathues, T.H., Prettyman, P., Schenk, H.G., Sizemore, M.D., Rayman, C.T., Russell, C.T., 2020. Impact-driven mobilization of deep crustal brines on dwarf planet Ceres. Nat. Astron. https://doi.org/10.1038/s41550-020-1168-2.

Ruesch, O., Platz, T., Schenk, P., McFadden, L.A., Castillo-Rogez, J.C., Quick, L.C., et al., 2016. Cryovolcanism on Ceres. Science 353, aaf4286.

Scully, J.E.C., Schenk, P.M., Buczkowski, D.L., Williams, D.A., Pasckert, J.H., Duarte, K. D., Romero, V.N., Sori, M.M., Landis, M.E., Castillo-Rogez, J.C., Quick, L.C., Sizemore, H.G., Neesemann, A., Schmidt, B.E., Raymond, C.A., Russell, C.T., 2020. Formation of the bright faculae in Ceres' Occator crater via long-lived brine effusion in a hydrothermal system. Nat. Commun. https://doi.org/10.1038/s41467-020-15973-8.

Simpson, F., Bahr, K., 2005. Practical Magnetotellurics. Cambridge Univ. Press.

Sonett, C.P., 1982. Electromagnetic induction in the moon. Rev. Geophys. Space Phys. 20, 411–455.

Sonett, C.P., Smith, B.F., Colburn, D.S., Schubert, G., Schwartz, K., 1972. The induced magnetic field of the moon: conductivity profiles and inferred temperature. Proc. Lunar Planet. Sci. 3rd, Geochem. Cosmochem. Acta 3, 2309–2336.

Telford, W.M., Geldart, L.P., Sheriff, R.E., 1990. Applied Geophysics, 2nd ed. Cambridge Univ. Press, Cambridge.

Wait, J.R., 1970. Electromagnetic Waves in Stratified Media. Pergamon, p. 1970.

Weidelt, P., 1972. The inverse problem of geomagnetic induction. Z. Geophys. 38, 257–289.